remote sensing

MDPI

Letter

Can InSAR Coherence and Closure Phase Be Used to Estimate Soil Moisture Changes?

Yusuf Eshqi Molan * and Zhong Lu

Roy M. Huffington Department of Earth Sciences, Southern Methodist University, Dallas, TX 75275-0395, USA; zhonglu@smu.edu

* Correspondence: yeshqimolan@smu.edu

Received: 25 March 2020; Accepted: 8 May 2020; Published: 9 May 2020

Abstract: We studied the influence of the statistical properties of soil moisture changes on the Interferometric Synthetic Aperture Radar (InSAR) coherence and closure phase to determine whether the InSAR coherence and closure phase can be used to estimate soil moisture changes. We generated semi-synthetic multi-looked interferograms by pairing n real single-looked pixels of an observed SAR image with n synthetic single-looked pixels. The synthetic SAR data are generated from the real SAR data by applying soil moisture changes with a pre-defined mean and standard deviation of changes. Our results show that the diversity of soil moisture changes within the multi-look window gives rise to decorrelation, a multi-looked phase artifact, and a non-zero phase triplet. The decorrelation and closure phase increase by enlarging the diversity of soil moisture changes. We also showed that non-soil moisture changes can lead to larger decorrelations and closure phases. Furthermore, the diversity of phase changes, decorrelation, and closure phases are correlated with land cover type. We concluded that the closure phase and coherence are independent of the magnitude of soil moisture changes and are inappropriate tools to estimate soil moisture changes. Coherence, however, can be used as a proxy for soil moisture changes if the diversity and magnitude of soil moisture changes within a multi-looked pixel are strongly correlated.

Keywords: synthetic aperture radar; soil moisture; closure phase; soil moisture diversity; coherence

1. Introduction

InSAR can remotely sense mm to cm-scale surface deformation [1–3]. InSAR has been used successfully to map surface deformations associated with different mechanisms, such as landslides, sinkholes, volcanism, subsidence, and permafrost [4–8]. Two SAR images of the same area with the same looking angle taken at different times can be used to generate an interferogram. After removing topographic phase, orbital, and atmospheric phase artifacts, the phase of an interferogram represents the deformation between two images in the line of sight direction. Between the two image acquisitions of an interferogram, however, the soil moisture may have also changed. The change in water content leads to changes in the InSAR phase and SAR intensity [9]. This in turn can influence the inferred deformation and potentially affect InSAR coherence.

In many agricultural and environmental studies, soil moisture plays a key role [10–12]. In addition, some ground movements associated with terrestrial processes have a close relationship with soil moisture changes. For example, rapid snowmelt or heavy precipitation can trigger sudden landslides [13]. Groundwater conditions can be indicated by soil moisture condition [14]. Additionally, soil moisture is closely related to permafrost thawing and deformation [6–8].

Many studies have been introduced to estimate soil moisture changes using the InSAR phase and SAR intensity [15–21]. However, soil moisture estimation using the InSAR phase has encountered difficulties and uncertainties. The spatial variability of soil moisture, unlike deformation, is complex [22].

In many cases, soil moisture varies abruptly; for example, across the boundaries of two agricultural fields. The temporal variability of soil moisture is also complex due, for example, to precipitation and seasonal effects [22]. In addition, the phase and intensity contribution of non-soil moisture changes cannot be easily distinguished from the soil moisture signal. Despite these difficulties, complex SAR images have been used to estimate soil moisture [16,17,22].

In order to avoid the difficulties in estimating soil moisture using the InSAR phase, some studies have recently introduced approaches to estimate soil moisture using the closure phase. By assuming that the closure phase comprises contributions from the magnitude of soil moisture changes, Zwieback et al. [23] tried to establish approaches to estimate soil moisture using the closure phase and InSAR coherence. The closure phase (also known as the phase triplet) is the combination of three interferograms generated from three SAR images. The phase of the single-looked interferogram pairing the first and the third SAR images equals the summation of the phases of the two intermediate single-looked interferograms. This means that a non-zero phase triplet does not exist in single-looked pixels [24]. For multi-looked pixels, however, the closure phase has non-zero values [23–25]. Some studies have discussed the possible causes of non-zero phase triplets. De Zan et al. [16] argued that non-zero phase triplets could occur due to the interference of different scatterer populations with independent phase behaviors. The authors associated the closure phase to the changes in the water content of soil and vegetation. Additionally, Zwieback et al. [17] argued that deformations do not cause non-zero phase triplets; the authors suggested that non-random effects of decorrelation noise, non-zero spatial baselines, and the change in dielectric constant can potentially cause phase inconsistency [16,17].

In contrast to the hypothesis that the magnitude of changes contributes to the closure phase [23,25], a new study showed that the closure phase is independent from the magnitude of changes [24]. Using analytical and statistical approaches, Molan et al. [24] studied the effect of the statistical properties of the phase and intensity of single-looked pixels on multi-looked phase and coherence. The authors showed that the closure phase is related to the heterogeneity of phase and intensity changes and is independent of the magnitude of changes. In this letter, we study the influence of soil moisture changes on the closure phase and coherence of multi-looked pixels. We aim to determine whether the closure phase or InSAR coherence can be used to estimate soil moisture changes.

To study the relationship between soil moisture changes and InSAR coherence and the closure phase, we generated semi-synthetic interferograms with variable soil moisture changes between the images. Using an analytical soil moisture model [9], the soil moisture values were converted to their corresponding phase and intensity changes. The phase and intensity changes were applied to the real pixels to generate synthetic pixels. Finally, semi-synthetic interferograms were generated using the real and synthetic pixels. The results from synthetic data showed that the multi-looked phase artifact, decorrelation, and closure phase increase by increasing the standard deviation of soil moisture changes within the multi-look window. We show that, compared to soil moisture changes, non-soil moisture changes can lead to larger decorrelation and closure phase values. To confirm the results of synthetic data, we used phase and coherence images generated from real SAR images of the Advanced Land Observing Satellite (ALOS) Phased Array type L-band Synthetic Aperture Radar (PALSAR) over two study areas in Idaho and Oregon. We also show that the heterogeneity of phase changes, decorrelation, and the closure phase are correlated with each other and with land cover type. We conclude that, in general, the closure phase and InSAR coherence are independent of the magnitude of soil moisture changes and are inappropriate tools to estimate soil moisture changes.

The rest of this letter is structured as follows: Section 2 describes the method of generating semi-synthetic interferograms; Section 3 provides the results generated from synthetic and real SAR images; Section 4 provides a discussion of the results; and finally, conclusions appear in Section 5.

2. Materials and Methods

To investigate the effect of the statistical characteristics of soil moisture changes on InSAR coherence and the closure phase, we exploit semi-synthetic interferograms. The first image of a semi-synthetic interferogram $\boldsymbol{u}_1$ is a real single-looked SAR image containing $p.q = n$ pixels. The second image $\boldsymbol{u}_2$ is synthetic data generated from real data by applying a change vector $\Delta\boldsymbol{u}_{1,2}$

$$\boldsymbol{u}_{\mathrm{j}} = \left[u_j^{(1)}, u_j^{(2)}, \ldots, u_j^{(n)}\right]', \mathrm{j} = 1, 2 \tag{1}$$

The intensity and phase changes of the change vector, respectively, are

$$\Delta\boldsymbol{dB} = f_{dB}(\boldsymbol{M_v}) + \Delta\boldsymbol{dB}_{ns}\ \Delta\boldsymbol{\theta} = f_{\theta}(\boldsymbol{M}_v) + \Delta\boldsymbol{\theta}_{ns} \tag{2}$$

where $\boldsymbol{M}_v$ is the vector of soil moisture changes between the real and synthetic images.

$$\boldsymbol{M_v} = \left[m^{(1)}, m^{(2)}, \ldots, m^{(n)}\right]' \tag{3}$$

In the equations above, $f_{\theta}(\boldsymbol{M_v})$, and $f_{dB}(\boldsymbol{M_v})$ are the soil moisture-dependent phase and intensity changes, respectively. $\Delta\boldsymbol{\theta}_{ns}$ and $\Delta\boldsymbol{dB}_{ns}$ indicate the phase and intensity changes associated with non-soil moisture changes between the two images, which in general include mechanical deformations, other artifacts, and noise.

Previous studies suggest a linear relationship between SAR intensity changes and soil moisture changes [26]. Additionally, a linear relationship between soil moisture changes and phase changes has been reported in the studies in which statistical approaches have been conducted [17]. Thus far, few analytical and statistical approaches have been introduced to quantify the relationship between soil moisture and SAR intensity or phase [18,27–35]. The studies generally model either phase or intensity. In this letter, we use the analytical model developed by Molan and Lu [9]. The model uses Mie equations and successfully quantifies soil moisture-induced changes in the InSAR phase and SAR intensity; this approach models soil as an attenuating dielectric medium with a collection of discrete coarse scatterers embedded in a background. The signal of a focused single-looked pixel, in the model, is [9]:

$$u = \sum_{i=1}^{N} e^{-j2kR} t_{1,2}\ t_{2,1}\ s_i\ e^{-2\int_0^z \frac{\alpha}{\cos(\theta_r)}dz'} e^{-j2(k_0 y_i \sin(\theta_r))} e^{-2j\int_0^z \beta\cos(\theta_r)dz'} W_a(x_i) W_r(y_i\sin(\theta_r) - n\cos(\theta_r) z_i) \tag{4}$$

where u is the signal of the single looked pixel—i.e., the total signal from all scattering pointsθ_r is the refracted angle, $t_{i,j}$ is the transmission coefficient of amplitude from medium i to medium j [26], R is the range of the pixel, k_0 is the free air wavenumber, and s_i is the amplitude of the scattered wave by the scatterer. Additionally, W_a and W_r are the slant range and azimuth resolution functions for the single scatterer located at $(x_i,\ y_i,\ z_i)$. The refraction of the soil medium is n. The absorption and phase constants of soil are, respectively, α and β. Figure 1 shows the modeled phase and intensity changes calculated using Equation (4). Without loss of generality, we assume that the soil background is loam that contains silt, clay, and sand. It also contains gravels with the grain size (r_p) of 2.65 cm and volume fraction (f_s) of 1.0%.

Using Equations (2) and (4), we can generate a synthetic image from a real image and a synthetic image with pre-defined soil moisture changes. The real image has n single-looked pixels. The soil moisture differences between the real and the synthetic image $\boldsymbol{M}_v$ are a random vector with pre-defined average Δm_v and standard deviation σ_{mv} values. Therefore, one soil moisture change Mv_i is associated to each of the single-looked pixels in the first image $u_1^{(i)}$. The soil moisture changes are converted to the equivalent phase and intensity changes using Equation (4). Then, the phase and intensity changes are applied to $u_1^{(i)}$ to generate $u_2^{(i)}$. After creating the synthetic image, an interferogram can be

generated using the real and synthetic images. Therefore, by applying different values to the average and standard deviation of soil moisture changes and calculating the resulting phase and coherence changes, we can assess the effect of the statistical properties of soil moisture changes on InSAR phase and coherence. To compare the influence of soil moisture change with the effect of non-soil moisture changes, we first assume that the non-soil moisture changes are negligible. Then, we generate the second type of interferograms that have both soil moisture and non-soil moisture changes.

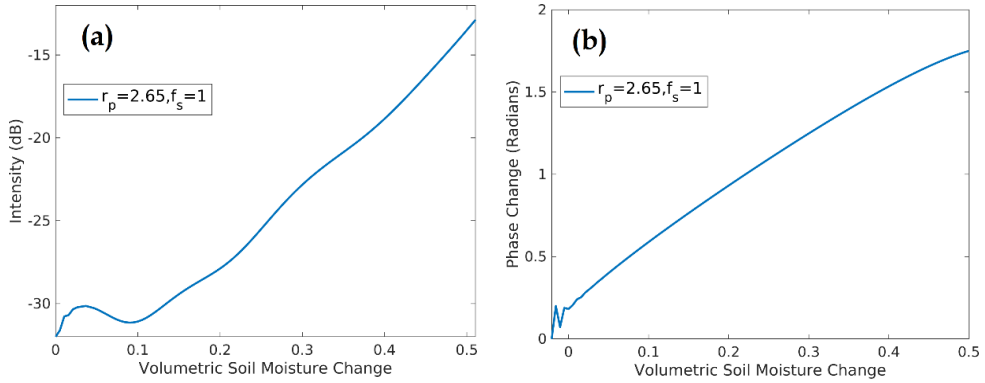

Figure 1. Intensity (**a**) and phase (**b**) changes of the soil. r_p is the radius of the larger grains (main scatterers) and f_s is the fractional volume of larger grains.

3. Results

3.1. Synthetic Data

The interferometric phase and coherence have an angle and magnitude of

$$\gamma = \frac{E\left[\boldsymbol{u}_1 \boldsymbol{u}_2^*\right]}{\sqrt{E\left[|\boldsymbol{u}_1|^2\right] E\left[|\boldsymbol{u}_2|^2\right]}} \tag{5}$$

To assess the effect of the statistical properties of soil moisture changes on the InSAR phase and coherence, two types of interferograms are generated. For the first type of interferogram, non-soil moisture changes are assumed to be zero. This means that $\Delta \boldsymbol{dB}_{ns}$ and $\Delta \boldsymbol{\theta}_{ns}$ in Equation (2) are zero and we obtain

$$\Delta \boldsymbol{dB} = f_{dB}(\boldsymbol{M_v}) \Delta \boldsymbol{\theta} = f_{\theta}(\boldsymbol{M_v}) \tag{6}$$

The intensity and phase changes associated with soil moisture changes—i.e., $f_{dB}(\boldsymbol{M_v})$ and $f_{\theta}(\boldsymbol{M_v})$—are calculated using Equation (4). Then, $\boldsymbol{u}_2$ is calculated by applying the phase and intensity change to $\boldsymbol{u}_1$, and finally, an interferogram is generated using $\boldsymbol{u}_1$ and $\boldsymbol{u}_2$. The average soil moisture changes of 0.05, 0.15, and 0.25 with the standard deviation in the range of 0.01–0.13 were applied between the two images to generate interferograms. For each case with the same average and standard deviation, 1000 interferograms were generated. Figure 2 illustrates the phase and coherence of the generated interferograms. In Figure 2, each point on the solid phase lines is the average phase of 1000 interferograms with a specific Δm_v and σ_{mv}. The same-color dashed lines show the average ± standard deviation of multi-looked phases of the interferograms. The average interferometric coherence values for those interferograms are also shown in Figure 2.

As stated previously, we considered zero non-soil moisture changes between the images to assess the influence of soil moisture changes of the InSAR coherence and closure phase. Now, we generate the second type of semi-synthetic interferograms by applying non-soil moisture changes ($\Delta \boldsymbol{dB}_{ns}$ and $\Delta \boldsymbol{\theta}_{ns}$) in addition to the soil moisture changes. Soil moisture changes lead to phase and intensity changes of SAR images. In general, the phase and intensity values increase along with increasing soil moisture (see Figure 1). In other words, dielectric constant changes due to soil moisture changes cause correlated

phase and intensity changes. Unlike soil moisture changes, the phase and intensity changes of non-soil moisture changes are assumed to be uncorrelated.

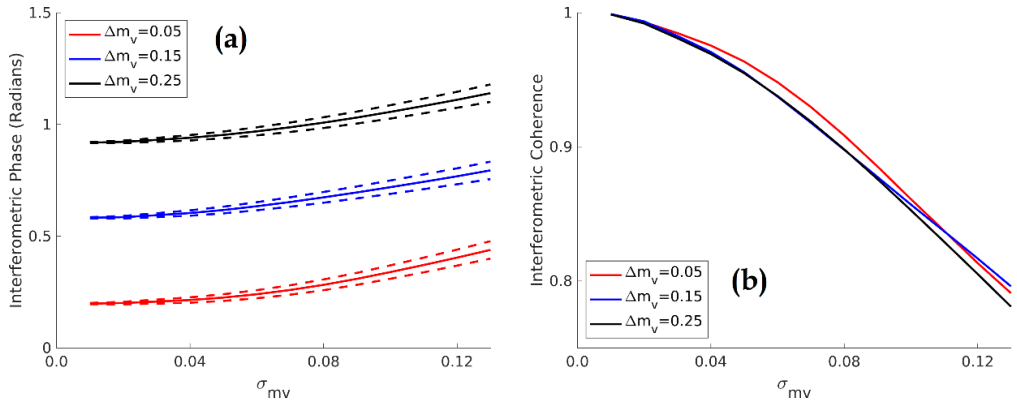

Figure 2. The phase (**a**) and coherence (**b**) changes due to the change in the average and standard deviation of soil-moisture changes.

In the second type of interferogram, which include both soil moisture and non-soil moisture changes, the average phase and intensity of non-soil moisture changes are considered to be zero. The standard deviations of the phase and intensity changes are 4 dB and 0.75 radians, respectively. The soil moisture changes of the second type of interferograms are identical to the soil moisture changes of the first type. The multi-looked phase and coherence values are shown in Figure 3. Similar to the first type of interferograms, we generated 1000 interferograms with the same average and standard deviation of changes for each case. Note that the influence of non-soil moisture changes is demonstrated by the larger distance between the average plot (solid phase line) and the average ± standard deviation plot (dashed phase lines). The coherence plot of non-soil moisture cases is shown in Figure 3, which dropped from 1.0 to 0.68 at $\sigma_{mv} = 0$.

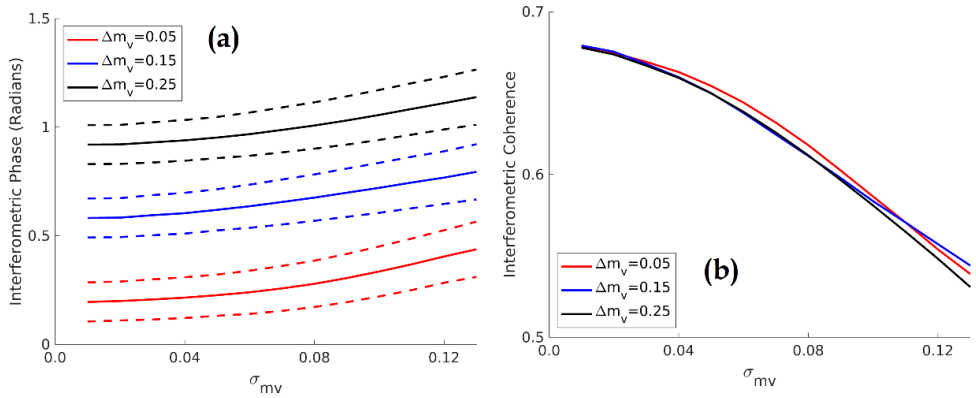

Figure 3. The phase (**a**) and coherence (**b**) changes due to the change in the average and standard deviation of soil-moisture changes and zero-mean random non-soil moisture change.

Three images can generate three mutual interferograms and one phase triplet, which is calculated by subtracting the phase of the interferogram pairing the first and the last images from the summation of the phases of the two intermediate interferograms [16,24]

$$\ddot{\varnothing}_{i,j,k} = \varnothing_{i,j} + \varnothing_{j,k} - \varnothing_{i,k} \tag{7}$$

We have used a pair of one real image and one synthetic image to generate the interferograms. Now, we can use one real image and two synthetic images to generate a closure phase image. We use

the same strategy applied in the previous section to generate the semi-synthetic interferograms. Figure 4 shows the closure phases generated using six different combinations of soil moisture changes. In Figure 4, each point on the image is the average value of 1000 closure phases with specific $\Delta m_{v,1}$, $\Delta m_{v,2}$, $\sigma_{mv,1}$, and $\sigma_{mv,1}$ values.

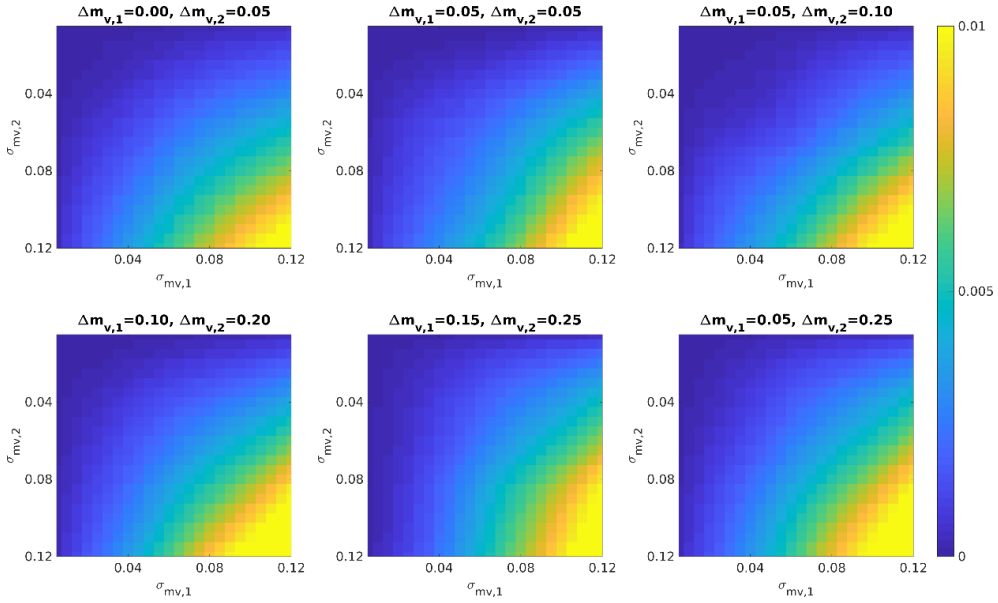

Figure 4. Closure phase (in radians) due to different combinations of soil moisture changes.

The results in Figure 4 were generated by assuming negligible non-soil moisture changes. The second type of closure phases were generated by applying both soil moisture and non-soil moisture changes between the images. We assumed that the non-soil moisture changes induce zero-mean phase and intensity changes with the standard deviations of 4 dB and 1.0 radian, respectively. The results of the second type of closure phases are shown in Figure 5.

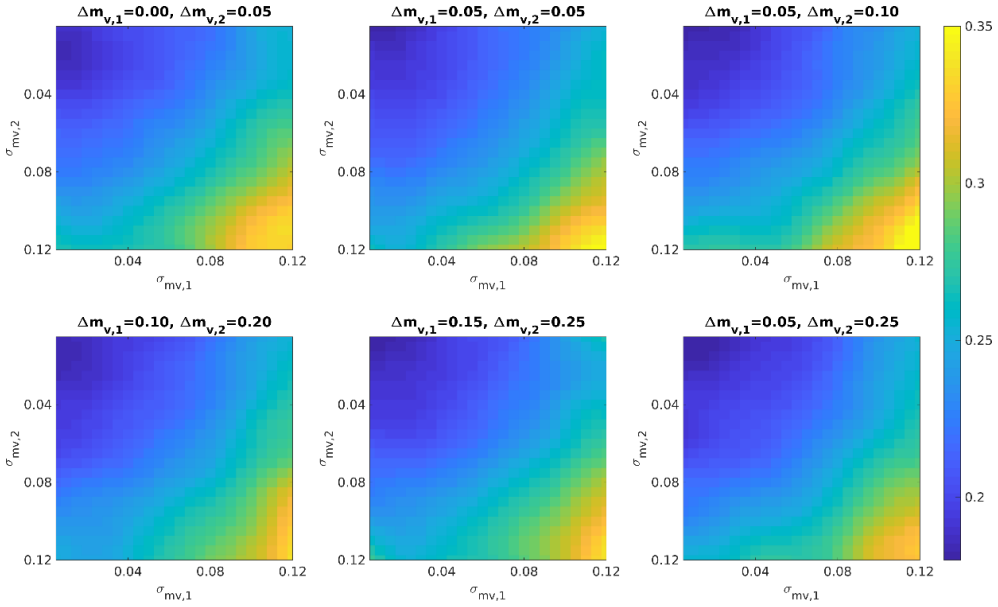

Figure 5. Closure phase (in radians) due to different combination of soil moisture changes and zero-mean random non-soil moisture change.

3.2. Real Data

Our results from synthetic data showed that the InSAR coherence and closure phase are functions of the standard deviation of soil moisture changes between images. Now, we use real SAR data over two areas in Oregon and Idaho to evaluate the results generated from the synthetic data. To this end, over each area, three co-registered single looked complex (SLC) images (the first three images in Tables 1 and 2) of the L-band ALOS PALSAR have been used to generate multi-looked interferograms with nine and four looks in azimuth and range, respectively. To simulate and remove the topographic phase from the interferograms, the Shuttle Radar Topography Mission (SRTM) Digital Elevation Model (DEM) with a 1 arc-second spatial resolution was used. The images over the area in Idaho are from ascending orbital path 208 and frame 860, and the images over the area in Oregon are from ascending orbital path 215 and frame 830. The data are in the fine beam and horizontal–horizontal (HH) polarization mode. Over each study area, from the three co-registered SLC images, three multi-looked interferograms and three coherence images were generated. In addition, for each study area, three circular standard deviation images S_c [36]—one for each interferogram—were generated. The circular standard deviation of a multi-looked pixel is calculated by

$$S_c = \sqrt{-2\ln\left|\sum_{i=1}^{n}\exp\left(j\theta_i\right)\right|} \tag{8}$$

where i is the number of the single-looked pixel, n is the total number of single-looked pixels in the multi-looked window, and θ_i is phase change of the pixel i. For each area, the three multi-looked interferograms were used to produce a closure phase image. Figures 6a and 7a show closure phase images. Similarly, the three circular standard deviation images were used to generate a standard deviation root mean square (RMS) image:

$$RMS_s = \sqrt{\frac{1}{3}\left({S_{c,1}}^2 + {S_{c,2}}^2 + {S_{c,3}}^2\right)} \tag{9}$$

Table 1. The date (yyyy-mm-dd) of the single looked complex (SLC) images over the study area in Idaho.

No.	Date	No.	Date	No.	Date	No.	Date
1	2007-07-05	4	2009-07-10	7	2010-05-28	10	2010-10-13
2	2007-08-20	5	2009-10-10	8	2010-07-13	11	2011-02-28
3	2007-11-20	6	2010-04-12	9	2010-08-28		

Table 2. The date (yyyy-mm-dd) of the SLC images over the study area in Oregon.

No.	Date	No.	Date	No.	Date
1	2007-08-01	2	2007-12-17	3	2008-03-18

Figures 6b and 7b show the standard deviation RMS images. The three coherence images were also used to generate the average coherence image R. Figures 6c and 7c show the average decorrelation images; i.e., 1-R.

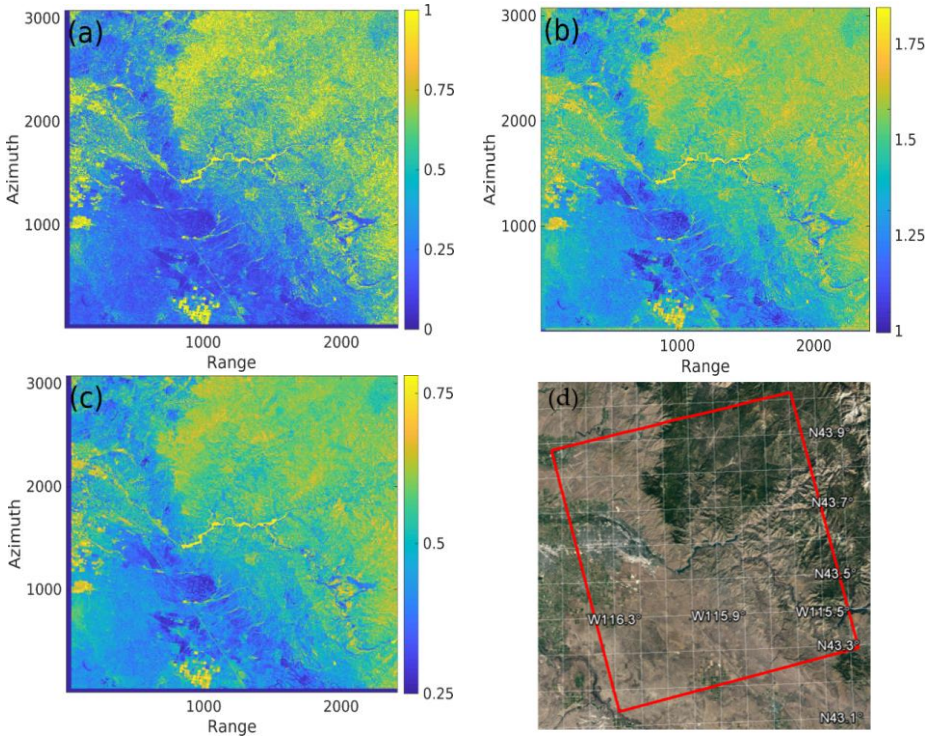

Figure 6. (**a**) Closure phase (in radians), (**b**) root mean square (RMS_s) of phase changes (in radians), and (**c**) average decorrelation over the study area in Idaho. (**d**) The red box on the optical image outlines the study area.

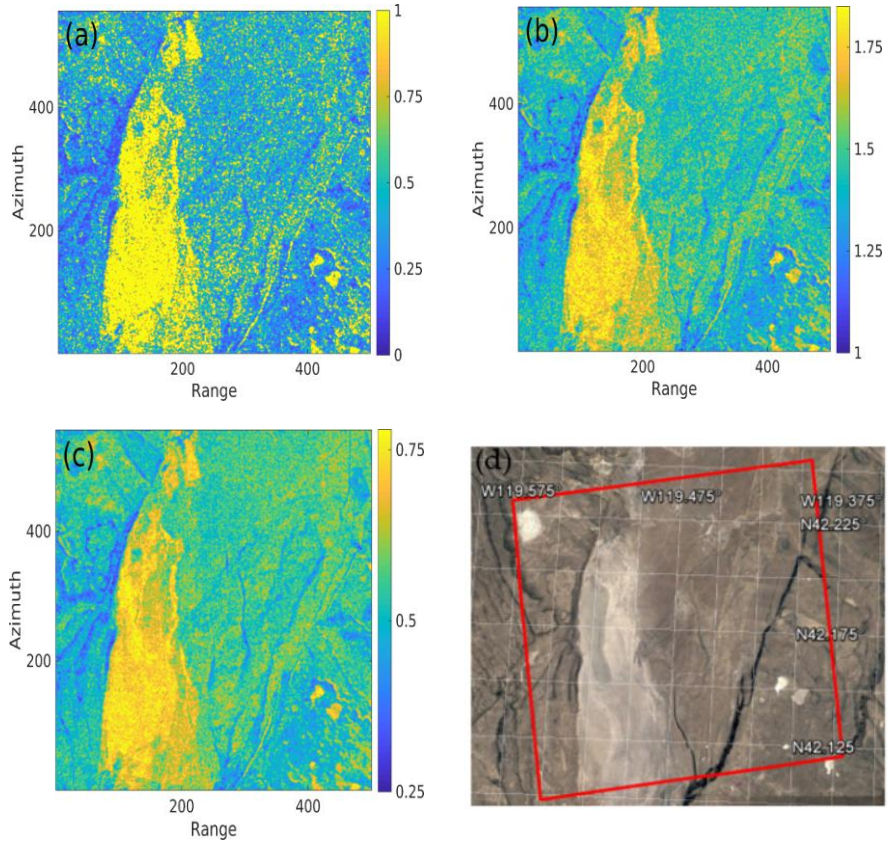

Figure 7. (**a**) Closure phase (in radians), (**b**) RMS_s of phase changes (in radians), and (**c**) average decorrelation over the study area in Oregon. (**d**) The red box on the optical image outlines the study area.

4. Discussion

Due to the strong effects of decorrelations and noises, single-looked interferograms are noisy. Multi-looking, which averages adjacent pixels in complex interferograms, improves phase reliability by reducing noise [37,38]. It has been shown, however, that the statistical properties of phase and intensity changes within a multi-look window influence the interferometric phase and coherence [24]. Molan et al. [24] showed that InSAR coherence and the closure phase are associated with the heterogeneity of phase and intensity changes. In this letter, we assessed changes in the InSAR phase, coherence, and the closure phase due to changes in the statistical properties of soil moisture changes using semi-synthetic interferograms. Our results indicate that a non-zero standard deviation of soil moisture changes within a multi-look window leads to decorrelation and non-zero closure phase. Regarding this, we discuss here whether the InSAR phase, coherence, and closure phase can be used for soil moisture estimation.

4.1. Soil Moisture-Induced Multi-Looked Phase Artifact and Non-Zero Phase Triplet

A multi-looked InSAR phase has been used for soil moisture estimation. The multi-looked interferometric phase includes contributions from physical changes as well as the statistical properties of the phase and intensity of single-looked pixels [24]. In the case of soil moisture changes between two multi-looked pixels, the average and standard deviation of soil moisture changes contribute to physical and statistical phases, respectively.

The results in Figure 2 illustrate the average interferometric phase $\varnothing$, physical phase $\varnothing_p$, statistical phase ($\varnothing_s = \varnothing - \varnothing_p$), and phase diversity. The solid and dashed lines, respectively, show the average and standard deviation of the interferometric phases. The physical phase $\varnothing_p$ in Figure 2 is the interferometric phase at $\sigma_{mv} = 0$ (the first point on the solid line), at which the statistical phase ($\varnothing_s$) is zero. The average statistical phase $\varnothing_s$ is the phase difference between interferometric phase $\varnothing$ (the solid line) and the physical phase $\varnothing_p$ (the first point on the solid line).

In Figure 2, we can see that the average statistical phase increases by increasing the standard deviation of soil moisture changes. However, soil moisture-induced phase diversity—i.e., the standard deviation—is negligible. The similar behavior of the average interferometric phase and statistical phase can be seen in Figure 3, which illustrates the results of non-soil moisture cases. Additionally, the diversity of interferometric phases increases by increasing the standard deviation of soil moisture and non-soil moisture changes. However, non-soil moisture changes lead to a larger diversity of phase changes compared to soil moisture changes (comparing the dashed lines in Figures 2 and 3).

Considering the contribution of the statistical phase, the InSAR phase can be potentially used for soil moisture estimation if the magnitude of the physical phase is significantly larger than the statistical phase. A thorough discussion of physical and statistical phase contributions to the multi-looked phase has been provided in [24]. However, as a general practical strategy, pixels with low coherence values should be avoided because low-coherence pixels are associated with larger statistical phases. In other word, both decorrelation and multi-looked phase artifacts (statistical phase) are functions of the standard deviation of changes [24].

The results in Figure 4 show that the closure phase is zero only when the σ_{mv} between images is zero. It is shown in Figure 4 that, regardless of the magnitude of soil moisture changes, the closure phase increases by increasing σ_{mv}. This indicates that the closure phase is independent of the magnitude of changes and is an inappropriate means to estimate soil moisture changes. Additionally, a comparison between soil moisture and non-soil moisture results, shown in Figures 4 and 5, respectively, shows that the closure phase values increase drastically by applying non-soil moisture changes. This is because non-soil moisture changes induce much larger phase diversity (see Figures 2 and 3). The practical implication of this is that the closure phase due to non-soil moisture changes can mask the soil moisture-induced closure phase. The general conclusion that one can make is that the closure phase, decorrelation, and phase diversity are smaller when the phase and intensity changes are correlated;

i.e., due to soil moisture-induced changes. The quantities increase drastically by increasing non-soil moisture changes; i.e., due to non-correlated phase and intensity changes.

4.2. Soil Moisture-Induced Decorrelation

The results show that coherence decreases by increasing the standard deviation of soil moisture changes. It should be noted that the small changes in coherence and the closure phase values of different soil moisture changes are due to the non-linear relationships between soil moisture and the phase and intensity of single-looked pixels (see Figure 1). Regarding the relationship between soil moisture changes and InSAR coherence, the main question is whether we can exploit InSAR coherence to estimate soil moisture changes. The results indicate that coherence, as with the closure phase, is a function of the standard deviation of changes and is independent of the magnitude of changes. Therefore, it cannot be directly used to estimate soil moisture. This conclusion is true except for those cases in which the magnitude and diversity of soil moisture changes (dielectric constant changes in general) are correlated. It should be noted that the uncertainty of soil moisture estimation for the cases in which the magnitude and diversity are correlated is related to the degree of association between the magnitude and diversity.

In our study area in Idaho, we show an example to assess the correlation between the magnitude and diversity of changes. To do this, for each multi-looked pixel, we calculated the correlation coefficient between the magnitude and diversity of the phase of single-looked pixels within the multi-looked window. Over the study area in Idaho, 11 co-registered SLC images of L-band ALOS PALSAR (Table 1) were used to generate 41 unwrapped multi-looked interferograms with 14 and seven looks in azimuth and range. The processing approach to generate unwrapped interferograms was explained above in Section 3. For each interferogram, one standard deviation of phase changes within multi-looked pixels were calculated. Therefore, each multi-looked pixel has 41 interferometric phase values and 41 standard deviation values. Finally, for each multi-looked pixel, the correlation coefficient between the interferometric phase values and the standard deviation values was calculated. Figure 8 illustrates the calculated correlation coefficient image; it shows that the correlation between the diversity and magnitude of phase changes is not strong—i.e., $|r| < 0.5$.

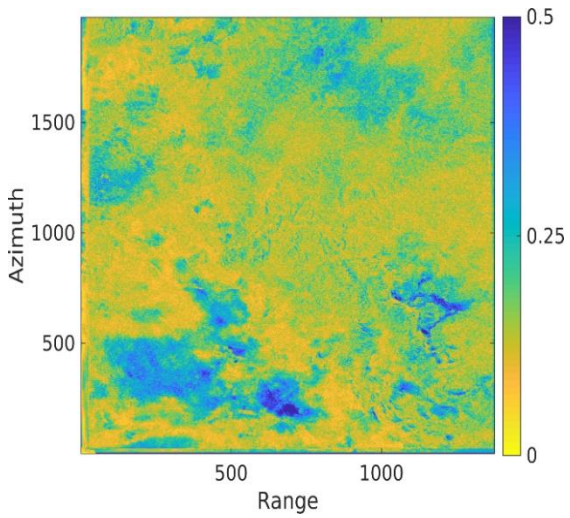

Figure 8. The correlation coefficient image over the study area in Idaho.

It should be noted that, even with a correlated magnitude and diversity of changes, soil moisture estimation using the closure phase, if not impractical, will suffer from high uncertainty in the results. This is because, unlike coherence, which is associated with the statistical properties of changes between one pair of images, the closure phase includes contributions from three interferograms, each with different statistical properties.

One other problem in using coherence to estimate soil moisture is related to the ambiguity in the orientation of soil moisture changes. An inferred soil moisture change can be assigned to both drying and wetting soils. This is even more complicated for the closure phase because it combines three interferograms. Furthermore, it should be noted that soil moisture estimation using InSAR coherence and the closure phase is even more challenging in practice. Coherence reduction and non-zero phase triplets due to non-soil moisture changes can hide the decorrelation and non-zero phase triplet of soil moisture changes. Figures 6 and 7 show optical images of our study areas. When comparing the closure phase values over different land cover types, we see very small values over bare soil with drastic increases over vegetated areas and agricultural fields (Figure 6). The standard deviation RMS and average decorrelation also show similar behaviors over different land cover types. The practical implication of this is that possible soil moisture signal in coherence and closure phase will be buried by the larger influence of vegetation.

However, the effect of vegetation is not the only obscuring influence on soil moisture-induced decorrelation and the closure phase. In Figure 7, which shows the results over the study area in Oregon, the decorrelation and closure phase are larger over unconsolidated sediments, as exemplified by the brighter area on the left side of the optical image. The area is covered by unconsolidated Quaternary surficial deposits [39]. Although not vegetated, higher decorrelation, closure phase, and diversity values can be seen over the area. This is because surficial deposits can be easily moved by surface water, leading to increased phase diversity.

5. Conclusions

Our analysis showed that InSAR coherence and the closure phase are functions of the diversity of soil moisture and non-soil moisture changes. The results of the synthetic data illustrated that non-soil moisture changes have a larger influence on decorrelation and closure phase. The results of the real data confirm that, compared to soil moisture changes, vegetation and surficial processes lead to much larger closure phase and decorrelations. It is also shown that closure phase and decorrelation are correlated with each other and with land cover type.

By considering the results of the synthetic and real data, we conclude that coherence and closure phase are not appropriate tools for soil moisture estimation. However, over sparsely vegetated areas and bare soils with stable surface deposits, coherence can be associated with soil moisture changes if a strong correlation exists between the magnitude and diversity of soil moisture changes and if coherence reductions caused by other environmental factors are negligible. To determine this association, studies should be conducted over different land cover types using intensive in-situ field data. Such investigations, however, may still suffer from high uncertainties in soil moisture estimations. Alternative methods such as the joint use of InSAR phase and SAR intensity changes should be considered for soil moisture estimation.

Author Contributions: Conceptualization, Y.E.M.; methodology, Y.E.M.; validation, Y.E.M. and Z.L.; writing—original draft preparation, Y.E.M.; writing—review and editing, Y.E.M. and Z.L.; supervision, Z.L.; funding acquisition, Z.L. All authors have read and agreed to the published version of the manuscript.

Funding: This research was funded by the NASA Earth Surface & Interior Program: NISAR Science Team, grant numbers 80NSSC19K1491, and NNX16AK56G and by the Shuler-Foscue Endowment at Southern Methodist University.

Conflicts of Interest: The authors declare no conflict of interest.

References

1. Massonnet, D.; Feigl, K. Radar interferometry and its application to changes in the Earth's surface. *Rev. Geophys.* **1998**, *36*, 441–500. [CrossRef]
2. Bürgmann, R.; Rosen, P.A.; Fielding, E.J. Synthetic Aperture Radar Interferometry to Measure Earth's Surface Topography and Its Deformation. *Annu. Rev. Earth Planet. Sci.* **2000**, *28*, 169–209. [CrossRef]

3. Simons, M.; Rosen, P. Treatise on Geophysics: Interferometric Synthetic Aperture Radar Geodesy. In *Geodesy*; Schubert, G., Ed.; Elsevier Press: Amsterdam, The Netherlands, 2007; Volume 3, pp. 391–446.
4. Lu, Z.; Dzurisin, D. InSAR imaging of Aleutian volcanoes: Monitoring a volcanic arc from space. In *Geophysical Sciences*; Springer Praxis Books: Chichester, UK, 2014; p. 390.
5. Ferretti, A.; Prati, C.; Rocca, F. Permanent scatterers in SAR interferometry. *IEEE Trans. Geosci. Remote Sens.* **2001**, *39*, 8–20. [CrossRef]
6. Molan, Y.E.; Kim, J.-W.; Lu, Z.; Wylie, B.; Zhu, Z. Modeling Wildfire-Induced Permafrost Deformation in an Alaskan Boreal Forest Using InSAR Observations. *Remote Sens.* **2018**, *10*, 405. [CrossRef]
7. Schaefer, K.; Liu, L.; Parsekian, A.; Jafarov, E.; Chen, A.; Zhang, T.; Gusmeroli, A.; Panda, S.; Zebker, H.A.; Schaefer, T. Remotely sensed active layer thickness (ReSALT) at Barrow, Alaska using interferometric synthetic aperture radar. *Remote Sens.* **2015**, *7*, 3735–3759. [CrossRef]
8. Liu, L.; Zhang, T.; Wahr, J. InSAR measurements of surface deformation over permafrost on the North Slope of Alaska. *J. Geophys. Res.* **2010**, *115*, F03023. [CrossRef]
9. Molan, Y.E.; Lu, Z. Modeling InSAR Phase and SAR intensity Changes Induced by Soil Moisture. *IEEE Trans. Geosci. Remote Sens.* **2020**. [CrossRef]
10. Hirschi, M.; Viterbo, P.; Seneviratne, S. Basin-scale water balance estimates of terrestrial water storage variations from ECMWF operational forecast analysis. *Geophys. Res. Lett.* **2006**, *33*, L21401. [CrossRef]
11. Liang, W.L.; Hung, F.X.; Chan, M.C.; Lu, T.H. Spatial structure of surface soil water content in a natural forested headwater catchment with a subtropical monsoon climate. *J. Hydrol.* **2014**, *516*, 210–221. [CrossRef]
12. Seneviratne, S.I.; Viterbo, P.; Luthi, D.; Schar, C. Inferring changes in terrestrial water storage using ERA-40 reanalysis data: The Mississippi River basin. *J. Clim.* **2004**, *17*, 2039–2057. [CrossRef]
13. Cardinali, M.; Ardizzone, F.; Galli, M.; Guzzetti, F.; Reichenbach, P. Landslides triggered by rapid snow melting, the December 1996-January 1997 event in Central Italy. In Proceedings of the EGS Plinius Conference, Cosenza, Italy, 1 January 2000; pp. 439–448.
14. Robinson, D.A.; Campbell, C.S. Soil Moisture Measurement for Ecological and Hydrological Watershed-Scale Observatories: A Review. *Vadose Zone J.* **2008**, *7*, 358–389. [CrossRef]
15. De Zan, F.; Parizzi, A.; Prats-Iraola, P.; López-Dekker, P. A SAR interferometric model for soil moisture. *IEEE Trans. Geosci. Remote Sens.* **2014**, *52*, 418–425. [CrossRef]
16. De Zan, F.; Zonno, M.; López-Dekker, P. Phase inconsistencies and multiple scattering in SAR interferometry. *IEEE Trans. Geosci. Remote Sens.* **2015**, *53*, 6608–6616. [CrossRef]
17. Zwieback, S.; Hensley, S.; Hajnsek, I. Assessment of soil moisture effects on L-band radar interferometry. *Remote Sens. Environ.* **2015**, *164*, 77–89. [CrossRef]
18. Zwieback, S.; Liu, X.; Antonova, S.; Heim, B.; Bartsch, A.; Boike, J.; Hajnsek, I. A statistical test of phase closure to detect influences on DInSAR deformation estimates besides displacements and decorrelation noise: Two case studies in high-latitude regions. *IEEE Trans. Geosci. Remote Sens.* **2016**, *54*, 5588–5601. [CrossRef]
19. Molan, Y.E.; Kim, J.-W.; Lu, Z.; Agram, P. L-Band Temporal Coherence Assessment and Modeling Using Amplitude and Snow Depth over Interior Alaska. *Remote Sens.* **2018**, *10*, 150. [CrossRef]
20. Hoekstra, P.; Delaney, A. Dielectric properties of soils at UHF and microwave frequencies. *J. Geophys. Res.* **1974**, *79*, 1699–1708. [CrossRef]
21. Hallikainen, M.; Ulaby, F.; Dobson, M.; El-Rayes, M.; Wu, L.K. Microwave dielectric behavior of wet soil—Part 1: Empirical models and experimental observations. *IEEE Trans. Geosci. Remote Sens.* **1985**, *23*, 25–34. [CrossRef]
22. Hensley, S.; Michel, T.; Van Zyl, J.; Muellerschoen, R.; Chapman, B.; Oveisgharan, S.; Haddad, Z.S.; Jackson, T.; Mladenova, I. Effect of soil moisture on polarimetric-interferometric repeat pass observations by UAVSAR during 2010 Canadian soil moisture campaign. In Proceedings of the IGARSS, Vancouver, BC, Canada, 24–29 July 2011; pp. 1063–1066.
23. Zwieback, S.; Hensley, S.; Hajnsek, I. Soil moisture estimation using differential radar interferometry: Toward separating soil moisture and displacements. *IEEE Trans. Geosci. Remote Sens.* **2017**, *55*, 5069–5083. [CrossRef]
24. Molan, Y.E.; Lu, Z.; Kim, J.-W. Influence of the statistical properties of phase and intensity on closure phase. *IEEE Trans. Geosci. Remote Sens.* **2020**. [CrossRef]
25. De Zan, F.; Gomba, G. Vegetation and soil moisture inversion from SAR closure phases: First experiments and results. *Remote Sens. Environ.* **2018**, *217*, 562–572. [CrossRef]

26. Barrett, B.; Dwyer, E.; Whelan, P. Soil moisture retrieval from active spaceborne microwave observations: An evaluation of current techniques. *Remote Sens.* **2009**, *1*, 210–242. [CrossRef]
27. Lu, Z.; Meyer, D. Study of high SAR backscattering due to an increase of soil moisture over less vegetated area: Its implication for characteristic of backscattering. *Int. J. Remote Sens.* **2002**, *23*, 1065–1076. [CrossRef]
28. Nolan, M.; Fatland, D.R.; Hinzman, L. DInsar measurement of soil moisture. *IEEE Trans. Geosci. Remote Sens.* **2003**, *41*, 2802–2813. [CrossRef]
29. Zhang, T.; Zeng, Q.; Li, Y.; Xiang, Y. Study on relation between InSAR coherence and soil moisture. *Proc. ISPRS Congr.* **2008**, *37*, 131–134.
30. Barrett, B.; Dwyer, E.; Whelan, P. The use of C- and L-band repeat pass interferometric SAR coherence for soil moisture change detection in vegetated areas. *Open Remote Sens. J.* **2012**, *5*, 37–53. [CrossRef]
31. Hajnsek, I.; Prats, P. Soil moisture estimation in time with DInSAR. In Proceedings of the IEEE IGARSS, Boston, MA, USA, 7–11 July 2008; Volume III, pp. 546–549.
32. Nesti, G.; Tarchi, D.; Rudant, J.-P. Decorrelation of backscattered signal due to soil moisture changes. *Proc. Int. Geosci. Remote Sens. Symp.* **1995**, *3*, 2026–2028.
33. Nesti, G.; Tarchi, D.; Despan, D.; Rudant, J.-P.; Bedidi, A.; Borderies, P.; Bachelier, E. Phase shift and decorrelation of radar signal related to soil moisture changes. In Proceedings of the 2nd ESA International Workshop on Retrieval of Bio- & Geo-Physical Parameter from SAR Data for Land Applications, ESTEC, Noordwijk, The Netherlands, 21–23 October 1998; pp. 423–430.
34. Rudant, J.-P.; Bedidi, A.; Calonne, R.; Massonnet, D.; Nesti, G.; Tarchi, D. Laboratory experiment for the interpretation of phase shift in SAR interferograms. In Proceedings of the FRINGE, Zurich, Switzerland, 30 September 1996.
35. Morrison, K.; Bennett, J.C.; Nolan, M.; Menon, R. Laboratory measurement of the DInSAR response to spatiotemporal variations in soil moisture. *IEEE Trans. Geosci. Remote Sens.* **2011**, *49*, 3815–3823. [CrossRef]
36. Zar, J.H. *Biostatistical Analysis*, 5th ed.; Prentice-Hall/Pearson: Upper Saddle River, NJ, USA, 2010.
37. Ferretti, A.; Fumagalli, A.; Novali, F.; Prati, C.; Rocca, F.; Rucci, A. A new algorithm for processing interferometric data-stacks: SqueeSAR. *IEEE Trans. Geosci. Remote Sens.* **2011**, *49*, 3460–3470. [CrossRef]
38. Goldstein, R.M.; Zebker, H.A.; Werner, C.L. Satellite Radar Interferometric: Two-dimensional phase unwrapping. *Radio Sci.* **1988**, *23*, 713–720. [CrossRef]
39. Walker, G.W.; Repenning, C. Reconnaissance Geologic Map of the Adel Quadrangle, Lake, Harney, and Malheur Counties, Oregon: Reston, Va., U.S. Geological Survey Interpretive Map I-446, 1965, Scale 1:250,000. Available online: https://ngmdb.usgs.gov/ngmdb/ngmdb_home.html (accessed on 2 January 2020).